Titanium ions dispersed into the ZrO2 matrix: Spectroscopic properties and photoinduced electron transfer

UNIVERSITÀ DEGLI STUDI DI TORINO

Titanium ions dispersed into the ZrO_2 matrix. Spectroscopic properties and photo-induced electron transfer

S. Livraghi, F. Olivero, M.C. Paganini, E. Giamello*

Dipartimento di Chimica IFM, Università di Torino and NIS, Nanostructured Interfaces and Surfaces Centre of Excellence, Via P. Giuria 7, I - 10125 Torino, Italy

* mariacristina.paganini@unito.it

In the present work different ZrO_2–TiO_2 mixed oxides, which are usually employed in photocatalytic processes and as catalytic support in heterogeneous catalysis, have been prepared via sol-gel synthesis or by wet impregnation. In the former case, as indicated by X-ray diffraction and Raman spectroscopy, solid solutions based on Ti ions diluted in the ZrO_2 matrix are formed in the range of Ti molar fraction from 0.01 to 0.15. These solids have interesting optical properties as the typical band gap transition of ZrO_2 undergoes a red shift proportional to the Ti loading which reach the remarkable value of 1.3 eV for the highest Ti concentration. Annealing under vacuum at various temperatures causes oxygen depletion with consequent reduction of the solid which shows up mainly in terms of formation of Ti^{3+} reduced centres which are characterized by a typical broad EPR signal similar to that observed in reduced TiO_2 (anatase). The ability of the mixed oxides in stabilizing surface superoxide anions ($O_2^{\bullet-}$) has also been investigated by EPR to obtain information both on the photoinduced charge separation process in the solids and on the state of thermally reduced systems. In the latter case the obtained evidence have some value to understand controversial problems concerning the TiO_2 reduced matrix.

KEYWORDS: dfbhngfhgfnhgmhgm

1. Introduction

Zirconium dioxide based materials such as pure ZrO_2 (Zirconia), cation stabilised ZrO_2 (PSZ Partially Stabilized Zirconia) or surface sulphated ZrO_2 (SZ) are widely employed as catalyst or as catalysts supports for a variety of reactions.[1] Furthermore zirconia demonstrates significant activity in heterogeneous photochemical processes such as photostimulated adsorption of several molecules like oxygen, hydrogen, and methane[2], photoreduction of CO_2 by means of different reduction agents[3,4] and water photolysis[5]. Basically three crystalline modifications of ZrO_2 are known; the monoclinic (m-ZrO_2) which is stable up to 1200 °C, the tetragonal (t-ZrO_2) which is stable up to 1900 °C and the cubic (c-ZrO_2) which is stable above 1900 °C. In addition, a metastable tetragonal form is also reported. The last type is stable up to 650 °C and its existence is attributed to stabilizing effects due to impurities and crystallite size effects[1].

High surface area ZrO_2 has low thermal stability and, when calcined at high temperatures, undergoes a phase transition from tetragonal to monoclinic accompanied by a drastic decrease in surface area. Therefore, several attempts have been made to improve the ZrO_2 thermal stability mainly by incorporation of other elements into the oxide lattice[6,7,8].

ZrO_2–TiO_2 mixed oxides have attracted much attention in recent years because they show both better thermal stability and modified surface acidity properties with respect to the bare ZrO_2[7,9] and they are therefore used, like the parent material, as catalysts and catalyst supports for various catalytic reactions[10,11] such as dehydrogenation[12,13] and isomerisation[14,15]. A relatively large number of studies have been thus devoted to the preparation of ZrO_2–TiO_2 mixed materials[16,17] under the form of powders or of thin films. Several examples of photocatalytic applications of this mixed oxide are available.[18,19,20,21,22,23]

Despite the interest for catalytic and photocatalytic applications of ZrO_2-TiO_2 mixed oxides a systematic characterization of the physico-chemical properties of these systems and to their surfaces is still lacking. We have therefore tackled a systematic work of preparation and characterization of these materials aiming to gain information on their electronic and optical properties as well as on their surface reactivity in dark and under irradiation. The present paper reports an investigation of ZrO_2–TiO_2 mixed oxides containing a relatively low fraction of TiO_2 (1-15 mol%) which have been prepared either by sol-gel synthesis or by wet impregnation. The synthesized materials have been characterized by several structural, optical, and magnetic techniques. A particular role is assumed, in our investigation, by Electron Paramagnetic Resonance (EPR).

EPR is the reference technique to study paramagnetic defects in solids and electron transfer processes leading to molecules in paramagnetic state[24,25]. In this work, in particular, paramagnetic centres related to the presence of Titanium ions in the lattice have been characterized. Furthermore

the electron transfer to surface adsorbed oxygen to give $O_2^{\bullet-}$ radical anions was investigated in dark for pre-reduced solids and, under irradiation, for the fully oxidized materials with the twofold purpose of monitoring the ability of the various solids in photo-stimulated electron transfer and of using the adsorbed $O_2^{\bullet-}$ as a probe of the surface sites present on this important but poorly characterized mixed oxide.

2. Experimental Section

All reactants employed in this work were purchased by Aldrich and used without further purification. Pure ZrO_2 has been synthesised via Sol-Gel from the reaction of a solution of Zirconium (IV) propoxide in isopropylic alcohol (molar ratio 1 : 4) with water (H_2O/alcohol molar ratio=1 :10) performed under constant stirring at room temperature. The gel so obtained was aged overnight at room temperature to ensure a complete hydrolysis and subsequently dried at 343 K. The dried material was heated at 773 K in air for two hours (heating rate 10 K/min). The same procedure was adopted to prepare three different titanium modified ZrO_2 (ZT samples) containing respectively 1, 5 and 15 mol% of titanium adding the appropriate amount of titanium (IV) isopropoxide in the starting alcoholic solution. The following labels will be adopted in the text to identify the different samples. Z for pure ZrO_2 and ZTn (where n indicates the titanium molar percentage) for titanium containing materials.

A second type of sample with 5 mol. % of TiO_2 in ZrO_2 has been prepared by wet impregnation. In the synthesis 1g of pure ZrO_2 (prepared as described above) was suspended in 30 ml of isopropylic alcohol with the suited amount of titanium (IV) isopropoxide for 24 hours under constant stirring at RT. The suspension was than slowly dried and eventually calcined at 773 K for two hours. This sample will be labelled with the abbreviation ZTi5.

X-Ray Diffraction (XRD) was performed by a Philips 1830 diffractometer using a K_α(Co) source and a X'Peret High-Score software for data handling. Micro-Raman spectra (acquisition range ……..) were acquired using an integrated confocal Raman system which includes a micro-spectrometer Horiba Jobin-Yvon HR800, an Olympus BX41 microscope and a CCD air-cooled detector operating at 203K. A polarised solid state Nd laser operating at 532.11 nm and 80 mW was used as the excitation source. Correct calibration of the instruments was verified by measuring the Stokes and anti-Stokes bands and checking the position of the Si band at 520.7 cm^{-1}.

Diffuse Reflectance UV-Visible spectra (DR UV-Vis) were recorded by a Varian Cary 5 spectrometer using a Cary win-UV/scan software. Electron Paramagnetic Resonance (EPR) spectra were run on a X-band CW-EPR Bruker EMX spectrometer equipped with a cylindrical cavity operating at 100 KHz field modulation. Photogeneration of superoxide species was performed

irradiating the samples with a 500 W mercury/xenon lamp (Oriel instruments) equipped with a IR water filter. Experiments were carried out putting the solid powder in Suprasil quartz glass tubes previously connected to a high vacuum pumping system which allows thermal activation. Thermal activation consisted in two steps. In the first one the sample was gradually heated until 773 K in dynamic vacuum condition for 30 minutes to eliminate all surface contaminants and to obtain a dehydroxilated surface. Since during thermal annealing reducible oxides loose oxygen in the second step the solid was re-oxidized at 773 K in O_2 (~ 40mbar) for two hours. In this way the starting material for each experiment is a fully dehydrated stoichiometric oxide.

3. Results and discussion

3.1 Structural and optical characterization.

Figure 1 shows the XRD diffraction patterns for pure ZrO_2 and for the ZrO_2/TiO_2 mixed materials prepared in this work. Bare zirconia is characterized by the presence of a relatively low amount of monoclinic phase beside the dominant tetragonal. All titanium modified ZrO_2 samples present the same two phases shown by bare ZrO_2. The monoclinic phase is less abundant in ZT15 sample (Fig 1e) than in the other ZT systems. No evidence of the presence of TiO_2 polymorphs is observed in the diffraction patterns of ZT mixed oxides. However since a weak peak at ~29° corresponding to the (101) plane reflection of TiO_2 (which is the most intense one for the Anatase polymorph) it could, in principle, be buried in the ZrO_2 diffraction pattern, we have further investigated the prepared materials using Raman spectroscopy.

Raman spectroscopy is an extremely powerful tool to determine the phase compositions in the case of many transition metal oxides[26] . In the present work this technique has been employed to verify the presence of TiO_2 crystals segregated in the mixed ZrO_2-TiO_2 system. The group theory allows, for tetragonal ZrO_2, six Raman active vibrational modes ($A_{1g} + 2B_{1g} + 3_{Eg}$) in the 100–800 cm^{-1} range, among which the peaks at ~145, ~270 and ~650 cm^{-1} can be assumed as characteristic of t-ZrO_2 [26,27].

For the monoclinic form (m-ZrO_2) the expected pattern is much more complex and 18 active Raman bands are predicted although not all always observable. Among them, a sharp doublet centred at ~180 cm^{-1}, and a peak at ~476 cm^{-1} can be assumed as the most sensitive analytical marks of the monoclinic phase[28,29]. Similarly, for TiO_2, the phases of the two most common polymorph, anatase and rutile, can be distinguished. Anatase shows six Raman active modes (A_{1g}, $2B_{1g}$, 3_{Eg}) which appear at ~144 cm^{-1}, ~399 cm^{-1}, ~519 cm^{-1} and ~639 cm^{-1}[30]. Fundamental modes at 143 cm^{-1}(B_{1g}), 447 cm^{-1} (E_g), 612 cm^{-1} (A_{1g}) and 826 cm^{-1} (B_{2g}) are usually adopted to identify the rutile polymorph[31]. The Raman spectra of all the samples investigated in the present work are

reported in Fig. 2. As in the case of XRD patterns all titanium modified samples basically show the same spectral features of the pure material.

The most significant peaks observed at 147 cm^{-1}, 272 cm^{-1}, 616 cm^{-1} and 647 cm^{-1} are due to the tetragonal phase of ZrO_2 while the doublet peaks at 176 cm^{-1} and 190 cm^{-1} and the peaks at 316 cm^{-1}, 382 cm^{-1}, 458 cm^{-1} and 477 cm^{-1} mark the presence of the monoclinic phase.

No traces of TiO_2 Raman modes is visible. Taking into account that there is a huge differences in the scattering properties of TiO_2 and ZrO_2, the absence of any TiO_2 mode, and in particular of the highly intense mode at 144 cm^{-1}, allows us to exclude the presence of segregated TiO_2 microcrystal in the system. Analyzing a mechanical mixture based on a tiny amount of TiO_2 in ZrO_2 a very intense peak at 144 cm^{-1} indeed shows up (see SI) to confirm our finding. We can thus confidentially assume that all ZT samples are true solid solutions of the two oxides.

DR-UV-Vis spectra of Ti-modified oxides and of pure ZrO_2 are compared in Fig. 3A. Titanium insertion in the ZrO_2 lattice causes a remarkable modification in the UV-Vis absorption properties. Bare ZrO_2 shows the typical absorption below 250nm due to the electronic transition from the valence band to the conduction band (Fig. 3A a) while titanium modified ZrO_2 samples show (Fig. 3 b-e) a light absorption extension toward 350nm. In particular two different effects show up depending on titanium loading (Fig. 3A b-d). The first one can be described in terms of a small red-shift of the ZrO_2 absorption band (observed for ZT1, ZT5 and ZTi5, Fig. 3A b,c,e), accompanied by the onset of an intense absorption (shoulder) at low energy with respect to the main absorption band.

Sample ZT15 corresponding to the higher Ti-loading (Fig. 3A e), exhibits a pronounced red shift (~ 1.3 eV) of the absorption band. In Fig. 3B the determination of the optical band gap absorption edge for pure ZrO_2 and ZT15 sample is reported. This was done assuming for the Ti modified ZrO_2 materials a direct allowed electron transition[32,33] as in the case of the bare zirconium dioxide.

3.2 EPR characterization of reduced solid.

Pure and titanium modified ZrO_2 show different paramagnetic entities. The as prepared samples, in particular, shows a weak signal with axial *g* tensor ($g_{\perp} \approx 1.98$ and $g_{//} \approx 1.95$.) due to a defect usually observed in ZrO_2 whose nature, at the moment, is not completely understood[34,35] (see SI). However, the most interesting paramagnetic signals appears when the oxides are thermally annealed (Fig. 4) at 773K in dynamic vacuum condition ($P < 10^{-4}$ mbar). In semiconducting oxides annealing in vacuo causes O_2 depletion with consequent partial reduction of the solid. Pure ZrO_2 and ZT samples show a different behaviour upon annealing. In the pure material the reduction

treatment causes the disappearance of the weak signal originally present and in parallel the formation of an isotropic signal at g=2.003 (Fig.4 a). In ZT samples (Fig.4 b-d) the same signal at g=2.003 is accompanied by the growth of a broad signal at higher field, due to a new paramagnetic centre, whose intensity is proportional to the titanium loading. The first signal at g=2.003 is usually associated to electrons trapped in the ZrO_2 matrix[35]. The electrons left in the solid after O_2 depletion, in fact, can be stabilized in trapping sites, most probably the vacancies formed along the same phenomenon . This is illustrated by the following reactions[36,37].

$$ZrO_2 \rightarrow ZrO_{2-x} + x/2O_2 + 2xe^- + xV_o'' \quad (1)$$

$$V_o'' + e^- \rightarrow V_o' \quad (2)$$

where we use, for the oxygen vacancies, the well known Kröger-Vink notation.

The second signal in Fig. 4 is characterized by a very broad axial line ($g_\perp$= 1.977, $g_{//}$=1.908) whose intensity is proportional to the Ti loading. This signal was never reported before for ZrO_2 matrix and, on the basis of its similarity with the signals usually observed in reduced TiO_2, is assigned to reduced Ti^{3+} centres in ZrO_2 matrix. The existence of Ti^{3+} centres in oxides different from TiO_2, however, is well documented in the literature[38,39,40].

When reduced samples are contacted with O_2 at RT (Fig. 5) an intense signal shows up at g > g_e which is due to adsorbed superoxide $O_2^{\bullet-}$ ions. This new EPR signal forms at the expenses of both signals present in reduced materials which thus correspond to two centres capable of electron transfer to molecular oxygen. However, since the intensity of the Ti^{3+} signal is by far the highest one, $O_2^{\bullet-}$ formation essentially occurs at the expenses of Ti^{3+}. The electron transfer at RT in the case of ZT15 sample (Fig. 5b) is not complete but a mild heating at 363 K is sufficient to practically eliminate the Ti^{3+} signals (Fig. 5c). Reaction 3 and 4 illustrate the above described process of electron localization of Ti^{4+} and electron transfer

$$e^- + Ti^{4+} \rightarrow Ti^{3+} \quad (3)$$

$$Ti^{3+} + O_{2(g)} \rightarrow O_2^{\bullet-}{}_{(ads)} + Ti^{4+} \quad (4)$$

Table 1 reports the spin Hamiltonian parameters of the various signals observed in the present work.

3.2.1 Features of Superoxide ($O_2^{\bullet-}$) spectra.

The EPR spectral features of $O_2^{\bullet-}$ species are determined by the presence of an unpaired electron in a π^* molecular orbital. The symmetry of the g tensor is therefore orthorhombic ($g_{xx} < g_{yy} << g_{zz}$), the z direction being that O_2 internuclear axis and the y direction that perpendicular to the

surface plane. The *g* tensor can be analyzed using the simplified equations $g_{xx} \approx g_e$, $g_{yy} = g_e + 2\lambda/E$ and $g_{zz} = g_e + 2\lambda/\Delta$, where λ is the oxygen spin-orbit coupling constant, E is the energy level separation between the σ molecular orbital and the highest occupied π^* orbital, and Δ is the energy separation between the two $2\pi^*$ antibonding orbitals due to the electric field generated by the metal cation M^{n+} at the adsorption site (Scheme 1 A)[41]. From the previous equations it can be seen that the g_{zz} component is the most sensitive to the electric field of the adsorbing site and can therefore be used as a probe of the surface electric field gradients. In particular, the g_{zz} reported for $O_2^{\bullet-}$ species adsorbed on ZrO_2 ($O_2^{\bullet-}$---Zr^{4+}) is about 2.030-2.034 while for the TiO_2 ($O_2^{\bullet-}$---Ti^{4+}) values in the range between 2019 and 2.026 are usually reported.[42]

In the present work, an $O_2^{\bullet-}$ signal with a g_{zz} component at $g_{zz} \approx 2.030$ was observed for pure ZrO_2 while in the case of ZT samples the signal exhibits a double feature in the g_{zz} spectral region. A similar resolution is not observed for g_{yy} and g_{xx}. On the basis of the previous observation the spectra recorded in the case of ZT mixed materials are the overlap of a signal due $O_2^{\bullet-}$ on Zr^{4+} (g_{zz}=2.032) with a second signal (g_{zz}=2.022) unambiguously due to $O_2^{\bullet-}$ adsorbed on top of Ti^{4+} ions. The two slightly different g_{zz} values (2.032-2.022) are originated by the different charge to radius ratio of the two tetravalent ions (Scheme 1B). The reported experiment indicates that, in principle, it is possible to distinguish the nature of the absorption site (Zr^{4+} or Ti^{4+}) at the surface of mixed systems.

The photosensitivity of the semiconducting oxide can be investigated by EPR monitoring the capability of the system to transfer electrons under irradiation to a surface adsorbed acceptor molecule. Irradiating with photons having energy compatible with the band gap value (250nm in the present case) electrons are promoted from the valence band (V.B.) to the conduction band (C.B.). Mobile electrons at the surface can be scavenged by the acceptor molecule. Using O_2 as acceptor, $O_2^{\bullet-}$ ions are formed which are monitored by EPR (reactions 5 and 6).

$$ZrO_2 + h\nu \rightarrow ZrO_2\ (h^+_{(VB)}\ ;\ e^-_{(CB)}) \qquad (5)$$

$$e^-_{(CB)} + O_{2(g)} \rightarrow O_2^{\bullet-}{}_{(ads)} \qquad (6)$$

The formation of the same radical ion therefore is used to monitor either the electron transfer from a reduced solid (Fig. 5) or the photo induced electron transfer.

Fig. 6A compares the $O_2^{\bullet-}$ spectra obtained irradiating three samples with U.V. light. In this case the g_{zz} value for both $O_2^{\bullet-}$ species is slightly higher than that observed on annealed samples probably due to small difference in the state of the adsorption site in the two cases.[43] Surface Zr^{4+} ions are, for all the three samples, the dominating absorption sites in the case of photoinduced electron transfer as indicated by the intensity of the g = 2.035 component in all spectra. This component is, in fact, dominant in the case of ZT15 sample (Fig. 6A, a) where a minor line at g

=2.025 (Ti^{4+}) is however still appreciable. When titanium concentration drops (ZT5, Fig. 6A, b) the component at g = 2.025 is too low to be visible. This result suggests that for ZT systems the surface composition roughly reflects that of the bulk. This is confirmed by the result of sample ZTi5 (Fig. 6A, c). For this inhomogeneous material, prepared by surface impregnation, titanium concentration at the surface is higher than that present in the solid solution having the same loading (spectrum b). For this reason a fraction of $O_2^{\bullet-}$ adsorbed on Ti^{4+} is clearly appreciable in this case.

While the stabilization of photogenerated $O_2^{\bullet-}$ roughly reflects the composition of the solid and of its surface, the same does not apply when $O_2^{\bullet-}$ is formed via electron transfer from the reduced solid (Fig. 6B). In this second case the role of Ti^{4+} becomes more important The comparison of the spectra obtained by the two methods on the same material (that with the highest Ti loading, ZT15) is done in Fig. 6B (spectra a and a') to clarify this point. In spectrum a' (obtained by adsorption of oxygen on the pre-reduced sample, see also Fig. 5) the ratio between $O_2^{\bullet-}$ adsorbed on Ti^{4+} and on Zr^{4+} is completely reversed with respect to spectrum a and the Ti^{4+}--- $O_2^{\bullet-}$ species dominates the spectrum. The effect is also appreciable for ZT5 though less clearly because of the low Ti loading.

The previous findings clearly point to a different behaviour of the surface in the stabilization of O_2^- which depends on the state of the surface itself: unperturbed, in the case of photoinduced electron transfer or modified, in the case of pre-reduction of the solid.. The difference can be explained recalling that the reduction by annealing in vacuo causes the formation of substantial amounts of Ti^{3+} ions (Fig. 4) in parallel with oxygen vacancies and that superoxide formation occurs essentially at the expenses of Ti^{3+} (Fig. 5). Since O_2^- tends to stabilize preferentially (though not exclusively) on to Ti^{4+} ions (Fig 6B, a') we can infer that the electron transfer directly occurs from a surface reduced Ti^{3+} ion to an oxygen molecule which remains adsorbed on top of the ion itself. The present results thus indicate that the wide Ti^{3+} signal reported in Fig. 4 and also observed in bare TiO_2 essentially corresponds to surface reduced centres.

The location of reduced centres in semiconducting oxides (in particular TiO_2) is an open question. In the present case the broad EPR signal between g= 1.977 and g = 1.908 , also present on bare TiO_2, and never clearly assigned seems clearly be due to reduced ions present at the surface. This observation will be likely useful in the discussion about reduced states in TiO_2.

The ability of ZT solids in the photoinduced charge separation has been evaluated in quantitative terms monitoring the amount of photoformed $O_2^{\bullet-}$ radical ions by spin counting. The result is shown in Fig. 7 which clearly show that the propensity for the electron transfer increases with increasing the titanium content of the solid, provided that this ion is homogeneously dispersed into the matrix (ZTn samples). In ZTi5 in fact the photoactivity is depressed with respect to ZT5.

The results reported in Fig. 7 nicely agree with the results of optical absorption (Fig. 3). The higher the red shift of the optical threshold , the higher the fraction of absorbed photons, the higher the amount of photoformed superoxide.

4. Conclusions

ZrO_2-TiO_2 mixed systems were prepared using two different methods. Sol-gel synthesis leads to the formation of homogeneous solid solutions of the two oxides (ZTn materials) at least till a molar fraction of 15% TiO_2 in ZrO_2. The wet impregnation of zirconium dioxide , as opposite, leads to quite inhomogeneous systems with higher concentration of titanium ions in the surface layers. ZTn systems have remarkable optical properties in that a red shift of the valence band to conduction band transition is observed which is proportional to the Ti content. Reduction of the solids preferentially lead to the formation of of Ti^{3+} centres which are mainly localized at the surface and whose EPR signal is the same observed on thermally annealed TiO_2 (anatase).

The photoformation of $O_2^{\bullet-}$ is also proportional to the Ti content and, in quantitative terms, directly depends on the extent of the red shift of the band gap transition. $O_2^{\bullet-}$ in this case is distributed unselectively on the Zr^{4+} and Ti^{4+} surface sites whereas, when generated, by oxygen contact with reduced solids, the adsorption preferentially takes place on titanium ions. The prepared solid solutions, which are finding applications in catalysis and photocatalysis, are therefore also excellent model systems to investigate the role of impurities in modifying the band structure of a solid and the phenomena related to charge separation by effect of irradiation.

Acknowledgement

The micro-Raman has been obtained with the equipment acquired by the Interdepartmental Center “G. Scansetti” for Studies on Asbestos and Other Toxic Particulates with a grant from Compagnia di San Paolo, Torino, Italy.

Supporting Information Available: Full description of the material. This material is available free of charge via the Internet at http://pubs.acs.org.

References.

[1] Yamaguchi, T. *Catal. Today* **1994**, 20, 199.
[2] Emeline, A.V.; Panasuk, A.V.; Sheremetyeva, N.; Serpone, N. *J. Phys. Chem. B.* **2005**, 109, 2785.
[3] Kohono, Y.; Tanaka, T.; Funabiki, T.; Yoshida, S. *Phys. Chem. Chem. Phys.* **2000**, 2, 530.
[4] Kohono, Y.; Tanaka, T.; Funabiki, T.; Yoshida, S. *Chem. Commun.* **1997**, 841.
[5] Sayama, K.; Arakawa, H. *J. Phys. Chem.* **1993**, 97, 531.
[6] Xu, Q.; Anderson, M.A. *J. Am. Ceram. Soc.* **1993**, 76, 2093.
[7] Zou, H.; Lin, Y.S. *Appl. Catal. A* **2004**, 265, 35.
[8] Kubo, K.; Hosokawa, S.; Furukawa, S.; Iwamoto, S.; Inoue, M. *J Mater. Sci.* **2008**, 43, 2198.
[9] Manrıquez, M.E.; López, T.; Gómeza, R.; Navarrete, J. *J. Mol. Catal. A* **2004**, 220, 229.
[10] Wang, Y.; Ma, J.; Zhou, W.; Zhu,Y.; Song, X.; Li, H. *App.l. Catal. A* **2004**, 227, 55.
[11] Liang, L.; Sheng, Y.; Xu, Y.; Wu, D.; Sun, Y. *Thin Solid Films* **2007**, 515, 7765.
[12] Chang, R.C.; Wang, I. *J. Catal.* **1987**, 107, 195.
[13] Fung, J.; Wang, I. *J. Catal.* **1991**, 130, 577.
[14] Arata, A.; Akutagawa, S.; Tanabe, K. *Bull Chem Soc Jpn* **1976**, 49, 390.
[15] Tanabe, K.; Yamaguchi, T. *Catal. Today* **1994**, 20, 185.
[16] Chary, K.V.R.; Sagar, G.V.; Naresh, D.; Seela, K.K.; Sridhar, B. *J. Phys.Chem. B* **2005**, 109, 9437.
[17] Conga,Y.; Lia, B.; Leia, B.; Li, W.; J. *Lumin.* **2007**, 126, 822.
[18] Kataoka, S.; Tompkins, D.T.; Zeltner, W.A.; Anderson, M.A. *J Photochem. Photobiol. A: Chem.* **2002**, 148, 323.
[19] Liu, S.W.; Song, C.F., Lu, M.K.; Wang, S.F.; Sun, D.L.; Qi, Y.X.; Xi, D.; Yuan, D.R. *Catal. Commun.* **2003**, 4, 343-346.
[20] Navio, J.A.; Colon, G.; Herrmann, J.M. *J. Photochem Photobiol A: Chem* **1997**, 108, 179.
[21] Hernadez-Alonso, M.D.; Tejedor-Tejedor, I.; Coronado, J. M.; M. Anderson, A.; Soria, J. *Catal. Today* **2009**, 143, 364.
[22] Hernandez-Alonso, M.D.; Coronado, J. M.; Bachiller-Baeza, B.; Fernandez-Garcia, M.; Soria, *J. Chem. Mater.* **2007**, 19, 4283.
[23] Zhou, W.; Liu, K. S.; Fu, H. G.; Pan, K.; Zhang, L. L.; Wang, L.; Sun, C.C. *Nanotechnology* **2008**, 19, 035610.
[24] Chiesa, M.; Giamello, E.; Che, M. *Chem. Rev.* **2010,** *110,* 1320.
[25] Chiesa, M.; Paganini M. C.; Giamello E.; Murphy D.M.; Di Valentin C.; Pacchioni G. *Acc. Chem. Res.*, **2006**, 39, 861.
[26] Morterra, C.; Cerrato G.; Meligrana G.; Signoretto M.; Pinna F.; Strukul G. *Catal. Lett.* **2001**, 73, 113.
[27] Naumenko, A.P.; Berezovska, N.I.; Biliy, M.M.; Shevchenko, O.V. *J. Phys. Chem. Solids* **2008**, 9, 121.
[28] Duan, G.; Yang, X.; Lu, A.; Huang, G.; Lu, L.; Wang, X. *Mat. Charact.* **2007**, 58, 78.
[29] Li, M.; Feng, Z.; Xiong, G.; Ying, P.; Xin, Q.; Li, C. *J. Phys. Chem. B* **2001**, 105, 8107.
[30] Choi, H.C.; Jung, Y.M.; Kim, S. B. *Vibrational Spectroscopy* **2005**, 37, 33.
[31] Swamy, V.; Muddle, B. C.; Dai, Q. *Appl. Phys. Lett.* **2006**, 89, 163118.
[32] Barton, D.G.; Shtein, M.; Wilson, R.D.; Stuart, S. L.; Iglesia, E. *J. Phys. Chem. B.* **1999,** 103, 630.
[33] Boldish,S. I.; White, W. B. *Am. Miner.* **1998**, 83, 865.
[34] Morterra, C.; Giamello, E.; Orio, L.; Volante, M. *J. Phys. Chem.* **1990**, 94, 3111.
[35] Occhiuzzi, M. D.; Dragone, C. R. *J. Phys. Chem. B* **2002**, 106, 12464.
[36] Ben-Michael, R.; Tonnhauser, D.S.; Genassar, J. *Phys Rev. B* **1991**, 43, 7395.
[37] Azzoni, C.B.; Paleari, A. *Phys Rev. B* **1991**, 44, 6848.
[38] Lombard, P. B.; Ollier, B. N.; Jouini, A.; Yoshikawa, A. *J. Crystal Growth* **2009**, 311, 899.

[39] Konovalova, T. A.; Li, S.; Polyakov, N. E.; Focsan, A. L.; Dixon, D. A.; Kispert L. D. *J. Phys. Chem. B* **2009**, 113, 8707.
[40] Corradi, G.; Meyer, M.; Kovacs, L.; Polgar, K. *Appl. Phys. B* **2004**, 78, 607.
[41] Anpo, M.; Che, M.; Fubini, B.; Garrone, E.; Giamello, E.; Paganini, M.C. *Top. Catal.* **1999**, 8, 189.
[42] Che, M.; Tench, A. *Adv. Catal.* **1984**, 32, 2.
[43] Carter, E.; Carley, A. F.; Murphy, D. M. *J. Phys. Chem. C.* **2007,** 122, 10630.

Material	g values	Assignment	Ref.
All materials in oxidized state	$g_{\perp}$= 1.98 $g_{//}$= 1.96	Defects in ZrO_2	34, 35
ZrO_2 and ZT1 (annealed in vacuo)	g_{iso}=2.003	Trapped electrons in O vacancies	35
ZT1-ZT15 (annealed in vacuo)	$g_{\perp}$= 1.977 $g_{//}$= 1.908	Ti^{3+} ions in ZrO_2 matrix	This work
ZT1-ZT15 (O_2 adsorption on annealed solids)	g_{zz}= 2.032 g_{yy}=2.009 g_{xx}=2.003	$O_2^{\bullet-}{}_{(ads)}$ on Zr^{4+}	34
	g_{zz}= 2.022 g_{yy}=2.009 g_{xx}=2.003	$O_2^{\bullet-}{}_{(ads)}$ on Ti^{4+}	42

Table Errore. Solo documento principale.**:** Spin Hamiltonian parameters of the EPR signals reported in the present work

Figure 1: X-ray diffraction patterns of: a) ZrO_2. b) ZT1. c) ZT5. d) ZTi5. e) ZT15. ▼Monoclinic. ● Tetragonal.

Figure 2: Raman spectra of ZT samples. a) ZrO_2. b) ZT1. c) ZT5. d) ZTi5. e) ZT15. Dashed line: tetragonal ZrO_2. Dotted line: monoclinic ZrO_2. t=tetragonal, m=monoclinic.

Figure 3: [A]: DR-UV-Vis spectra of ZT samples. a) ZrO_2, b) ZT1, c) ZT5, d) ZT15, e) ZTi5. [B]: Band Gap and optical absorption edge evaluation for ZrO_2. (a, a') and ZT15. (d, d').

Figure 4: EPR spectra of ZrO_2 and ZT samples after thermal annealing. a) ZrO_2 , b) ZT1, c) ZT5, d) ZT15

Figura 5: EPR spectra of ZT15 sample after: a) annealing in vacuo at 773K. b) successive contact with O_2. c) temperature increase in O_2 at 363K

Figure 6: A: EPR spectra of $O_2^{\bullet-}$ species generated at the surface of ZT samples upon U.V. irradiation. a) ZT15, b) ZT5, ZTi5. B: Magnification and comparison, for ZT15, of the EPR spectra of $O_2^{\bullet-}$ obtained by irradiation (a) and by adsorption on the pre-reduced solid (a').

Figure 7: Comparison of the $O_2^{\bullet-}$ species generated at the ZT samples surface upon U.V. irradiation of equal amount of material.

Scheme 1: A) Energy levels of the oxygen molecule and of the adsorbed $O_2^{\bullet-}$ radical ion.. B) Schematic view of the different absorption sites at the surface of ZT samples.

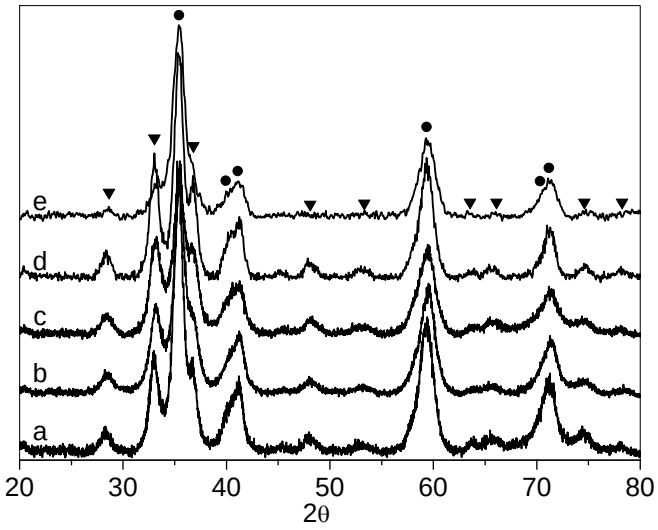

Figure 1:

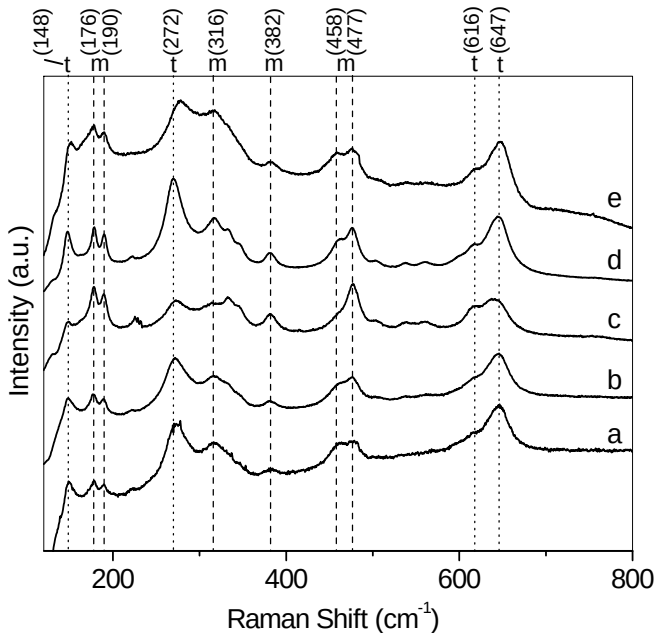

Figure 2:

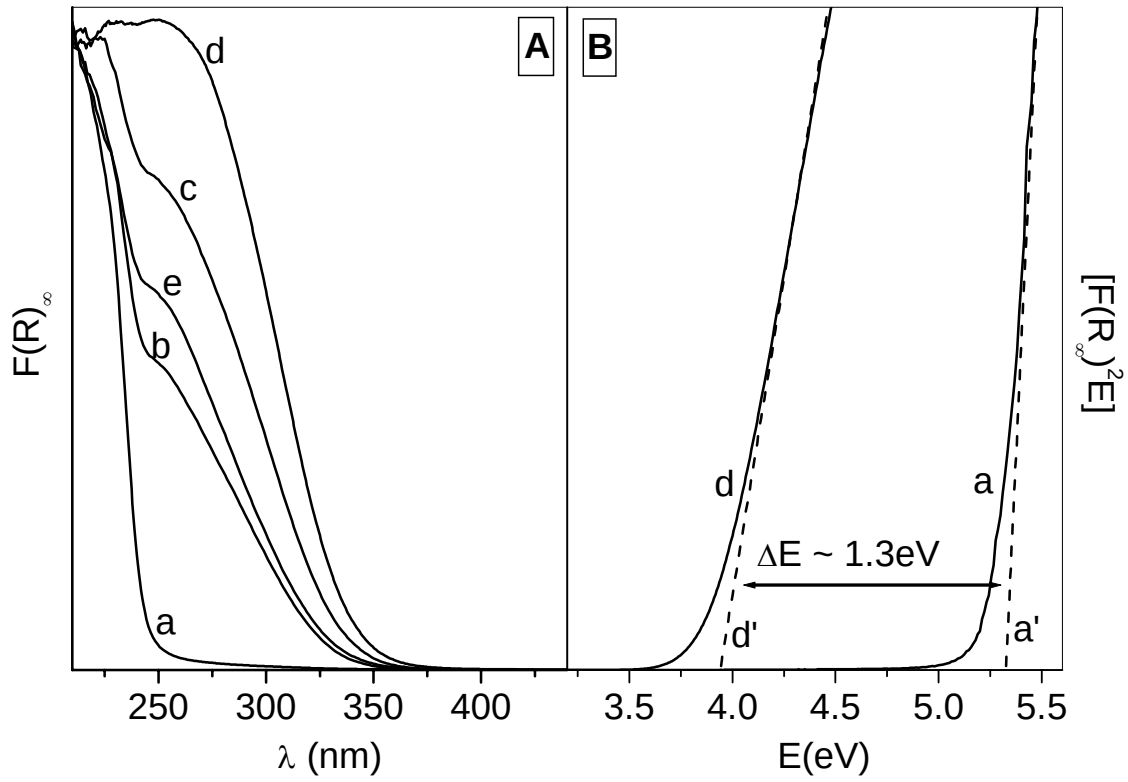

Figure 3:

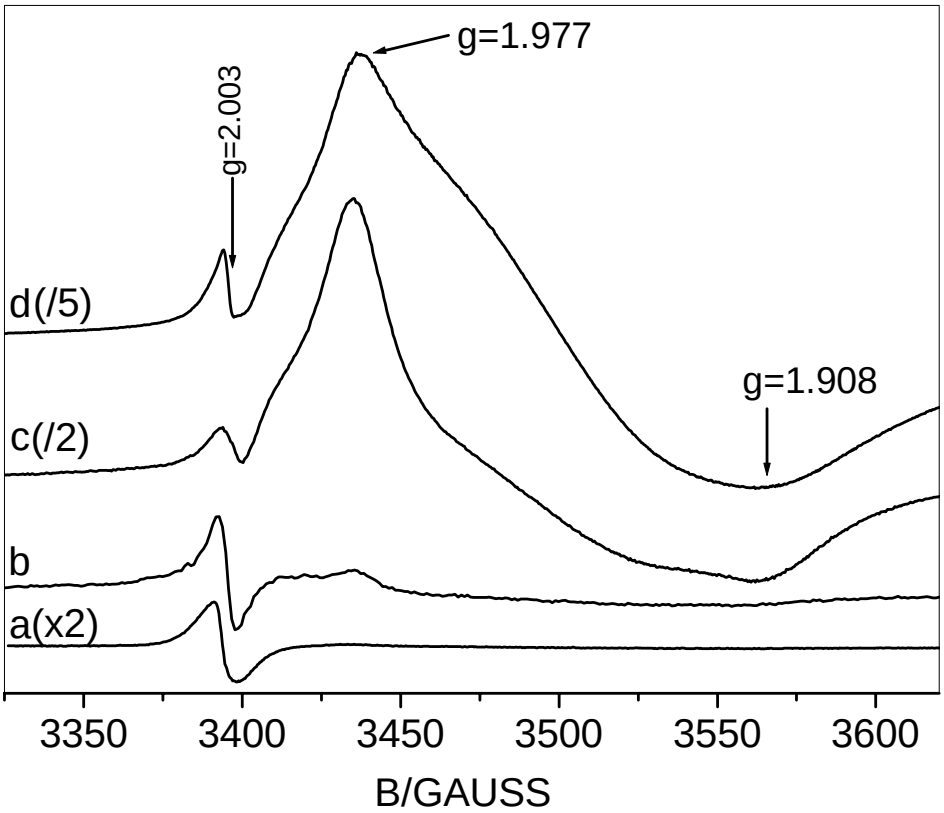

Figure 4:

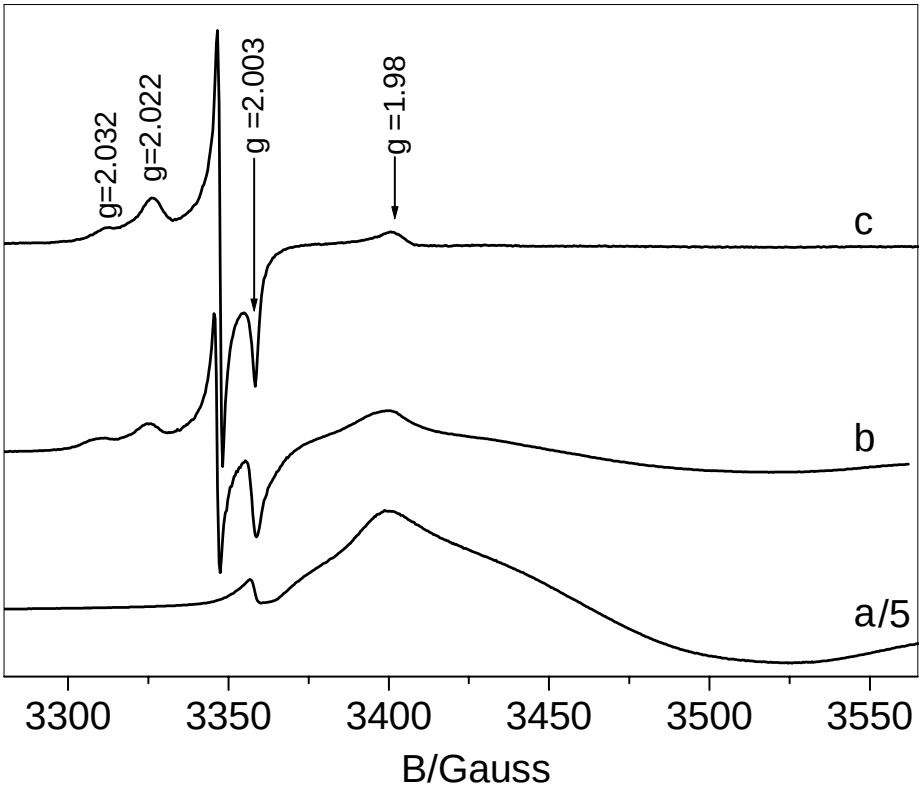

Figura 5:

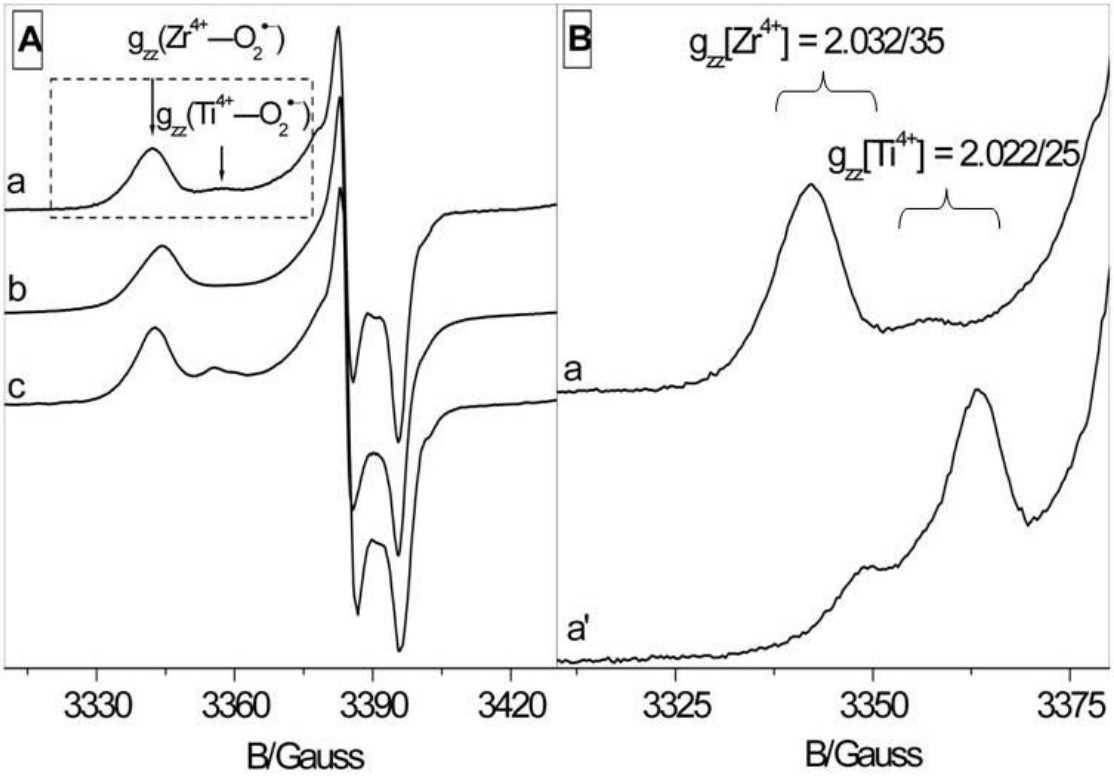

Figure 6:

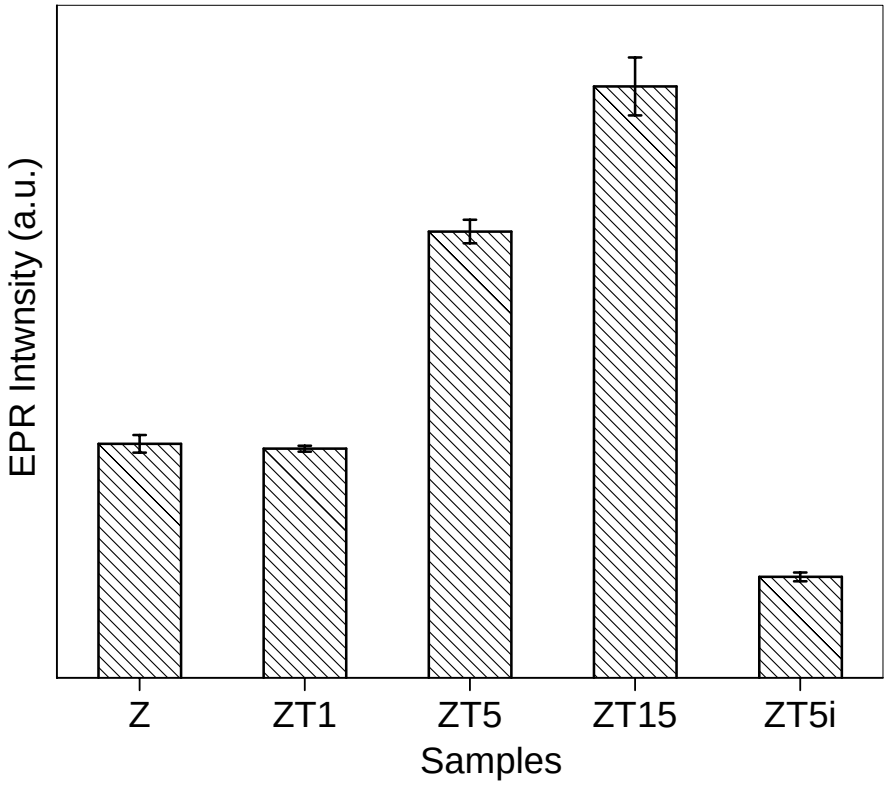

Figure 7:

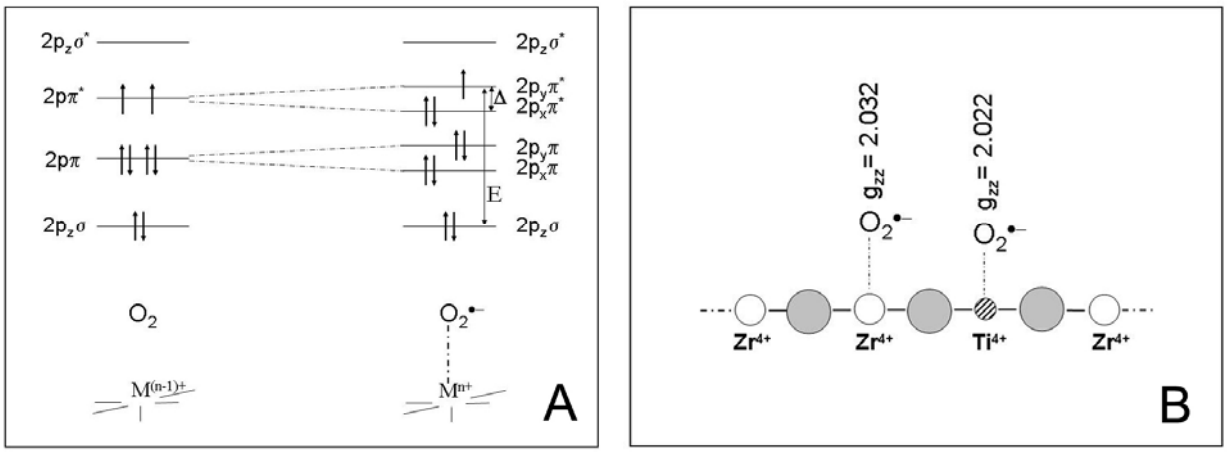

Scheme 1:

Table of Contents (TOC) Image